universe

MDPI

Review

The Missing Lead: Developments in the Lead (Pb) Discrepancy in Intrinsically *s*-Process Enriched Single Post-AGB Stars

Devika Kamath [1,2,*] and Hans Van Winckel [3]

[1] Department of Physics and Astronomy, Macquarie University, Sydney, NSW 2119, Australia
[2] Astronomy, Astrophysics and Astrophotonics Research Centre, Macquarie University, Sydney, NSW 2119, Australia
[3] Instituut voor Sterrenkunde, K.U. Leuven, Celestijnenlaan 200D bus 2401, B-3001 Leuven, Belgium; Hans.VanWinckel@kuleuven.be
* Correspondence: devika.kamath@mq.edu.au

Abstract: Lead (Pb) is predicted to have large over-abundances with respect to other *s*-process elements in Asymptotic Giant Branch (AGB) stars, especially of low metallicities. However, our previous abundance studies of *s*-process enriched post-Asymptotic Giant Branch (post-AGB) stars in the Galaxy and the Magellanic Clouds show a discrepancy between observed and predicted Pb abundances. For the subset of post-AGB stars with low metallicities the determined upper limits based on detailed chemical abundance studies are much lower than what is predicted. Recent theoretical studies have pointed to the occurrence of the *i*-process to explain the observed chemical patterns, especially of Pb. A major development, in the observational context, is the release of the GAIA EDR3 parallaxes of the post-AGBs in the Galaxy, which has opened the gateway to systematically studying the sample of stars as a function of current luminosities (which can be linked to their initial masses). In this paper, we succinctly review the Pb discrepancy in post-AGB stars and present the latest observational and theoretical developments in this research landscape.

Keywords: stars: AGB and post-AGB; stars: chemically peculiar; neutron-capture processes; Magellanic Clouds; Galaxy: stellar content; stars: abundances; techniques: spectroscopy

Citation: Kamath, D.; Van Winckel, H. The Missing Lead: Developments in the Lead (Pb) Discrepancy in Intrinsically *s*-Process Enriched Single Post-AGB Stars. *Universe* **2021**, *7*, 446. https://doi.org/10.3390/universe7110446

Academic Editor: Ana M. Heras

Received: 6 October 2021
Accepted: 10 November 2021
Published: 19 November 2021

1. Introduction

Primordial lead (Pb), comprising of the isotopes ^{204}Pb, ^{206}Pb, ^{207}Pb, ^{208}Pb, is believed to be created via the neutron-capture processes occurring in stars or their explosions [1]. The two main neutron-capture processes responsible for the creation of Pb are the slow neutron capture (*s*-process, e.g., [2–4] and references therein) and the rapid neutron capture (*r*-process, e.g., [5] and references therein). In astrophysics Pb is especially relevant because the double magic ^{208}Pb isotope marks an island of stability.

Neutron-capture processes are responsible for the production of most of the heavy elements in the mass region A $>$ 60. Starting typically from an iron seed, via a sequence of neutron captures and beta decays, the *s*-process synthesizes elemental isotopes. The astrophysical sites and physical conditions for the occurrence of these two processes are rather distinct. Although the occurrence of the *r*-process has long been associated with high neutron density environments ($n \geq 10^{20}$ cm^{-3}) such as those found in supernovae, more recent studies have also revealed possible sites such as mergers of neutron stars, neutron-star–black hole mergers, hypernovae, and accretion disk outflows related to the collapse of fast rotating massive stars (see [6] and for a review of *r*-process). The detection of a neutron-neutron star merger via its gravitational wave signal (GW170817) and the implication on the *r*-process production is one of the highlights of astrophysical research in 2017. The *r*-process usually synthesizes the most neutron-rich stable isotopes of each heavy element, with the abundance peaks for the *r*-process occurring near mass numbers A = 82 [elements selenium (Se), bromine (Br), and krypton (Kr)], A = 130 [elements

tellurium (Te), iodine (I), and xenon (Xe)] and A = 196 [elements osmium (Os), iridium (Ir), and platinum (Pt)].

On the other hand, the *s*-process, occurs over much longer timescales, and in environments with relatively lower neutron densities ($n \leq 10^{11}$ cm^{-3}) such that the less stable nuclei can undergo beta decay. Observational studies have shown that the astrophysical sites of the *s*-process mainly include stars on the AGB phase of their evolution (see [7–10] and references therein). At the end of helium- and carbon-burning in massive stars, elements from iron group seed nuclei on up to strontium (Sr) and yttrium (Y) are synthesized via the weak component of the *s*-process. In low-metallicity stars, the main component of the *s*-process produces heavy elements beyond Sr and Y, and up to Pb. The *s*-process chain is thus limited to the light *s*-process elements (i.e., ls elements) for moderate irradiations, while the heavy *s*-process elements (i.e., hs elements) are produced for increasing neutron irradiations. The ratio [hs/ls] is therefore an intrinsic indicator of the total neutron irradiation. When the neutron irradiation increases even further, the elements beyond the hs peak are produced up to the final product Pb. Each branch of the *s*-process reaction chain eventually terminates at a cycle involving Pb, bismuth (Bi), and polonium (Po).

As the neutron production in the *s*-process is thought to be largely dependent on primary nuclei (made by nucleosynthesis in the star itself) and hence independent of the initial metallicity, there are more neutrons available per iron seed and, hence at low metallicity Pb is predicted to have large over-abundances with respect to other *s*-elements (see [2,3,11,12] and references therein).

Strong Pb enhancements are indeed observed in extrinsically enriched metal-poor objects, which accreted mass from their companion, which passed through the thermally pulsing-AGB phase, but which is now a white dwarf [13]. However, not all metal-deficient objects with extrinsic enrichment show this strong Pb overabundance (e.g., [14,15]) in contrast to the predictions. To explain these abundance differences, alternate nucleosynthetic process, such as the intermediate neutron-capture process (i.e., *i*-process), have been postulated.

The *i*-process, an intermediate process to the *s*- and *r*-process, was postulated by [16]. The *i*-process is considered to operate at neutron densities intermediate to the *s*- and *r*-process (i.e., $n \leq 10^{14} - 10^{15}$ cm^{-3}, see [17–19] and references therein). This hypothesis gained popularity with the discovery of *r*/*s* stars (see [11,20]), and observational studies of carbon-enhanced metal-poor (CEMP) stars [21] with puzzling heavy element abundances, particularly of Ba and Eu. Theoretical studies by [11,22,23] have shown that the observed abundances of CEMP stars are best explained with a neutron-capture process that occurs with neutron densities similar to that proposed in the *i*-process. Furthermore, recent studies by [24] have shown that to explain the abundances observed in objects such as CEMP-rs stars, which collectively represent characteristic of extrinsic stars such as CEMP-s, CH, barium, and extrinsic S stars, the *i*-process plays a crucial role. It is considered that CEMP-rs stars can be explained as being polluted by a low-mass, low-metallicity thermally pulsing AGB companion experiencing *i*-process nucleosynthesis after proton ingestion during its first convective thermal pulses. One of the difficulties in the astrophysical interpretation of these abundances of CEMP stars is that the original donor of the enriched material is now a dim white dwarf the characteristics of which is hard to determine.

Our past studies (see [25] and references therein) of single intrinsic *s*-process rich post-AGB stars have provided therefore the perfect astrophysical laboratories to test our understanding of AGB nucleosynthesis, especially of the *s*-process and the *i*-process. Our studies [25,26] have revealed that the chemical patterns of single, low-metallicity ([Fe/H] < -0.7 dex) and likely low mass (<3.5 $M_{\odot}$) post-AGB stars in the Galaxy and especially in the Magellanic Clouds, enriched with carbon and *s*-process elements, show an interesting complexity. This subset of low-metallicity post-AGB stars show an underabundance of Pb (based on observationally derived upper limits) compared to the observationally derived abundances of other *s*-process elements, and compared to the theoretically expected values. This is very curious because the end product of the *s*-process nucle-

osynthesis chain is the double magic lead ^{208}Pb isotope, which is predicted to have large over-abundances with respect to other *s*-elements in metal-poor conditions (see [2,12,27] and references therein). On comparing the observations with dedicated AGB models (see Sections 3 and 4), we found indeed a strong discrepancy between the observed and predicted Pb over-abundances.

Until recently, we were confined to studying the abundance behavior of Pb for a wide range of initial metallicities—a key parameter for theoretical AGB models. We have not been able to systematically investigate the behavior of Pb as a function of initial mass—another key parameter for theoretical AGB models. This was due to the fact that the number of well-studied post-AGB stars in the Magellanic Clouds (for which we know accurate distances and hence luminosities and estimated initial masses) is limited (to around 5 objects of around 1–1.5 $M_{\odot}$). Additionally, the lack of accurate distances to the Galactic objects restricted the derivations of luminosities (and hence initial masses) to the larger sample of Galactic sources. With the release of the GAIA EDR3 parallaxes and distances [28], we have now successfully derived luminosities to the Galactic post-AGB stars, therefore opening the possibility to harness the hidden wealth of these objects. From a theoretical standpoint, developments in *i*-process nucleosynthesis have opened the doors to solving the Pb discrepancy problem. In this study, we succinctly review the Pb discrepancy in post-AGB stars and present the latest observational and theoretical developments in this research landscape.

2. Detecting Pb in the Photospheres of Post-AGB Stars

Post-AGB stars, the progeny of AGB stars, contain the products of AGB nucleosynthesis. During the post-AGB phase, the warm stellar photosphere makes it possible to quantify photospheric abundances for a very wide range of elements from CNO up to some of the heaviest *s*-process elements well beyond the Ba peak [29] that are brought to the stellar surface during the AGB phase. This is not possible with AGB stars since molecular veiling dominates their spectra [30]. Therefore, post-AGB objects can provide direct and stringent constraints on the parameters governing stellar evolution and nucleosynthesis, especially during the chemically rich AGB phase.

In this study, our focus is specifically on the abundances of Pb, so we present the tracers of Pb in the photospheres of post-AGB stars. Additionally, we constrain this study to intrinsically enriched post-AGB stars, as they are ideal tracers of the AGB nucleosynthesis that occurs during and the prior to their AGB phase. We suspect that these objects are either single or on very wide binaries [31].

Post-AGB stars typically are of late-G to late-A spectral types, with low log g values, and low metallicities (i.e., lower than the red giant stars in the host Galaxy). For the typical atmospheric parameters of the known single post-AGB stars in the Galaxy (e.g., [31] Kamath et al., 2021, to-be-submitted.), SMC (e.g., [32]), and LMC (e.g., [33,34]), there are only limited number of usable Pb lines in the optical spectrum. Additionally, the number of strong spectral lines decreases with increasing effective temperature for all elements.

Depending on the effective temperature of the sample stars and the total abundance, the Pb abundances are probed either using the strongest Pb I line at 4057.807 or Pb II line at 5608.853. As the Pb I line lies in a low S/N region with many blends and the Pb II line is generally very small so that it can be confused with noise in the spectrum, it is challenging to trace a clear Pb line feature. When a clear Pb line cannot be detected, spectral synthesis of the regions around the Pb lines need to be carried out and hence a complete set of elemental abundances is required. These abundances are then used to make detailed spectral synthesis in the regions of the strongest Pb lines, and subsequently the best constraints on the Pb abundances are derived. For the spectral synthesis of the Pb I, the spectral blends of unidentified lines at 4057.5 and 4058.9 are used to estimate the position of the continuum and a synthetic Pb I line is generated which fully incorporates the observed line feature at 4057.807. For the Pb II line at 5608.85, the continuum between 5606.3 and 5608 in combination with the blend at 5610.3 is used to estimate the position

of the continuum at 5608.853. The Pb II line lies in a spectral region where the continuum is affected by a blend of small unidentified spectral lines, ranging from 5608 up to 5610, therefore care must be taken to ensure that the feature is real. Owing to the challenges, some of which are presented above, it is often only possible to derive upper limits for the Pb abundances rather than well constrained abundances. More details on the spectral analysis using Pb lines are presented in [35] and the references therein.

3. Lead Abundances of *s*-Process Enriched Post-AGB Single Stars in the Galaxy and the Magellanic Clouds

To study the abundance behavior of Pb in intrinsically enriched stars, in our previous studies (e.g., [25,26]), we carried out systematic and detailed LTE abundance studies (with a focus on Pb) of the known sample of *s*-process enriched, single post-AGB stars in the Magellanic Clouds, and the Galaxy. The sample studied comprised of 1 object in the SMC [26], 5 in the LMC [26], and 14 objects in the Galaxy [25]. We note that one of the 14 Galactic objects (i.e., IRAS 17279-1119) was revealed to be in a binary system (see [25]). These studies [25,26] revealed that none of these intrinsically enriched single post-AGB stars are strong Pb producers-a stark contrast to theoretical predictions (see Section 4). The single post-AGB stars: 1 SMC object, 5 LMC objects, and 13 Galactic objects; together with their derived metallicities, [s/Fe], and upper limits for [Pb/hs] and [Pb/ls] are presented in Table A1 of Appendix A.

By studying objects in the Magellanic Clouds and the Galaxy, we were able to study the abundance behavior of Pb for a wide range of metallicities ($-2.0 <$ [Fe/H] < -0.5 dex). This resulted in a very important result: for higher metallicities of about [Fe/H] > -0.7 dex, the theoretical predictions from a suite of theoretical models (from [36–38]) are compatible with the observationally derived upper limits of the Pb abundances (as shown in Figure 14 of [25]). However, there exists an increasing discrepancy towards lower metallicities (i.e., [Fe/H] < -0.7 dex) where the upper limits are systematically lower that the predicted Pb abundances. For the benefit of the reader, we have reproduced Figure 14 of [25] in Table A1 of Appendix A. It is critical to note that in the studies of [25,26], we were unable to fully exploit the observational sample, initial mass estimates were only available for the 5 post-AGB stars in the Magellanic Clouds (where the distances, and hence luminosities and initial masses are well constrained). Stellar evolution and nucleosynthesis is heavily dependent on the initial mass. The lack of distances back in 2016, and hence luminosities of the Galactic objects stymied the estimation of their initial masses.

In our recent study (Kamath et al., 2021, to-be-submitted) we have used the Gaia EDR3 parallaxes to derive accurate luminosities and initial mass estimates to the full sample of single post-AGB stars in the Galaxy. These luminosities have opened a gateway to fully exploit the current sample of Galactic post-AGB stars. In this paper, we present the derived luminosities for all the Galactic objects considered (see Table A1 of Appendix A). We note that the error bars on the derived luminosities (see Table A1) represent the errors in the parallaxes which dominate the errors in the stellar parameters and photometric data that were used in the derivation of the luminosities. We refer the readers to Kamath et al., 2021, to-be-submitted, for full details on the procedure used to derive the luminosities and associated error bars. We also note that for some objects the derived luminosities are rather low and/or come with reasonable errors (see Object 1, 2, and 5 in Table A1). We are investigating the reason for these low luminosities, but it is beyond the scope of this study.

In Figure 1 we show the derived upper limits of [Pb/hs] for the sample of 19 stars (see Table A1) as a function of luminosity. Additionally, shown in the plot is the metallicity of the individual objects via a color table. The plot reveals that there is no obvious effect of luminosity (and hence initial mass) on the derived upper limits of the Pb abundances in *s*-process enriched post-AGB stars. However, this needs to be investigated in detail with dedicated AGB models tailored to individual objects. Additionally, our past studies have shown: (i) a correlation between [s/Fe] and [hs/ls] indicating the connection between strong neutron irradiations and the creation of heavy *s*-process elements, and (ii) the lack of correlation between neutron irradiation and metallicity (see Figure 15 of [25]).

As mentioned above, to fully understand these observational trends, comparisons need to be made with tailored state-of-the-art AGB evolution and nucleosynthesis models. With the new estimates of luminosities presented above, it is now finally possible to systematically compare the derived abundance results for a range of elements (e.g., CNO, Fe-peak, and *s*-process elements including derived upper limits for Pb) from post-AGB stars spanning a range of initial masses (from 1 to ∼3.5 $M_{\odot}$) and metallicity environments (i.e., in the Galaxy, SMC, and SMC) with theoretical predictions, thus improving our knowledge of the AGB nucleosynthesis and third dredge-up.

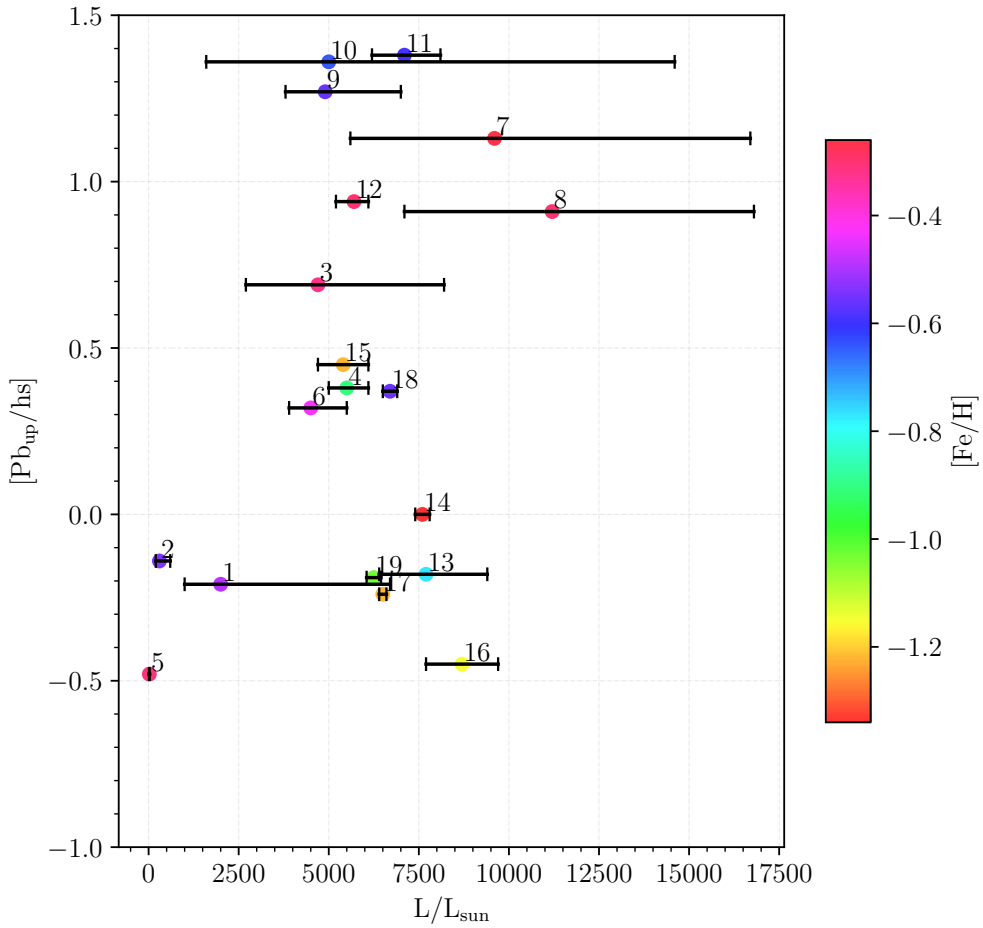

Figure 1. [Pb_{up}/hs] as a function of derived photospheric luminosities for the sample of post-AGB stars considered in this study. The color bar represents the metallicity ([Fe/H]) of the objects. See Section 3 for more details.

4. Current Theoretical Status

In our initial studies of Pb abundances of post-AGB stars [25,26,39], we compared the observational derived upper limits of the Pb abundances for the individual objects with dedicated stellar models of 1.5–2 $M_{\odot}$ with [Fe/H] ≈ −1.0. These models included: STAREVOL [36,40], Mount Stromlo models (MSE [38] and references therein), and the FRUITY models [41,42]. By and large, the models were based on a ^{13}C-pocket arising from diffusive overshooting at the base of the convective envelope during the third dredge-up. However, these models have problems reproducing the observed low Pb abundances in metal-poor stars. Additionally, these models also have problems in reproducing the observed spread in [hs/ls] of post-AGB stars at a given metallicity. Moreover, the C/O ratios and especially also the $^{12}C/^{13}C$ isotopic ratios are much higher than observed. These discrepancies point to missing physical ingredients and alternative processes in theoretical stellar models need to be investigated.

Our detailed chemical abundance studies have inspired a wave of new dedicated theoretical studies to investigate the Pb discrepancy. [4] explored modifications to the current scenario for the *s*-process in AGB stars to account for the Pb deficiency derived for the post-AGB stars in the Magellanic Clouds (i.e., Objects 14, 15, 16, and 17 of Table A1). These objects are of low metallicity ([Fe/H] ≈ -1.2) and low initial mass ($\approx$ 1–1.5 $M_{\odot}$). The authors tested different amounts and distributions of protons leading to the production of the main neutron source within the ^{13}C-pocket and proton ingestion scenarios. Two ^{13}C-pockets produced by two different constant proton abundances (Y_p) mixed into the intershell (i.e., $Y_p = 0.7 \times 10^{-4}$ and $Y_p = 1.05 \times 10^{-4}$) were adopted to match the determined Pb over-abundances. However, for these two cases, the full abundance patterns (especially the derived abundances of the elements in between Eu and Pb) could not be reproduced. Ref. [4] suggested that neutron-capture processes with neutron densities intermediate between the *s*- and the *r*-processes may provide a solution to this problem.

The Advent of the i-Process

The *i*-process represents an intermediate neutron-capture process midway between the *s*- and *r*-processes and mostly relies on the injection of protons in a convective helium-burning region (see [43] and references therein). The astrophysical site of the *i*-process is still debated, but theoretical studies (for e.g., [37,44]) using an AGB model with 1.5 $M_{\odot}$ at [Fe/H] = -2.4 and with a network of $\sim$700 isotopes have shown that *i*-process nucleosynthesis can take place during the early stages of the AGB phase, especially at low-metallicity and in low-mass stars. There has been significant progress in investigating several other *i*-process related astrophysical sites. For example, in the study by [45], the authors investigate the *i*-process nucleosynthesis by post-processing Rapidly Accreting White Dwarfs (RAWDs) models with $-2.6 <$ [Fe/H] < 0. Additionally, [19] explored *i*-process nucleosynthesis in CEMP stars and post-AGB stars using one-dimensional, single-zone nuclear-reaction network calculations at constant temperature and density, and with constant neutron densities.

Although the calculations presented in [19] do not exactly represent realistic stellar environments, they provide a great initial insight into the mechanisms potentially responsible for *i*-process in objects such as post-AGB stars. Since post-AGB stars are the centerpieces of our study we summarize the results from [19], who investigate the low derived upper limits of Pb abundances found in 7 post-AGB stars (Objects 4, 13, 14, 15, 16, 17, 19, Table A1). The objects chosen are of low-metallicity ([Fe/H] < -0.7) and low-mass ($\approx$ 1–1.5 $M_{\odot}$). This is in accordance with the fact that the upper limits for the Pb abundances of stars with [Fe/H] > -0.7 are compatible with predictions from appropriate AGB models (see Section 3). Ref. [19] report that the full abundance patterns and upper Pb limits of all 7 post-AGB stars can be fitted best by *i*-process calculations of neutron densities: $n = 10^{11}$ cm^{-3} and $n = 10^{12}$ cm^{-3} and integrated neutron exposures ($1.0 \leq \tau \leq 1.3$ mbarn^{-1} which translates to timescales in the range of 0.2 to 2.5 years). These values (of n and τ) sit at the lower end of the tested neutron densities and integrated neutron exposures and are lower than those required to reproduce the heavy element abundances (including Pb) for the lower-metallicity CEMP-i stars.

Stellar models under realistic conditions are required, however, to better understand the actual mechanisms responsible for *i*-process, including the 'where' and 'when' this process occurs. It is critical to understand the true extent and behavior of the entire neutron-capture process (i.e., *s*-process, *i*-process, and/or both) that occurs during the AGB and possibly post-AGB (via late He-shell flashes) phases.

5. Conclusions

As the expected end product of the *s*-process chain, the Pb abundance is sensitive to the different nucleosynthetic processes that occur during the AGB phase. Our chemical abundance studies [25,46] showed that the predicted Pb abundances for *s*-process enriched post-AGB stars, especially with [Fe/H] < -0.7 are too high, and difference between the

observationally derived upper limits for the Pb abundance and the predictions increases towards lower metallicities.

We note that in our observational studies [25,46], we do not consider non-LTE effects. [47] carried out non-LTE calculations for the Pb I line at 4057.807 for the Sun and for a set of stellar parameters characteristic of metal-poor stars in the range of $-2.95 <$ [Fe/H] < -0.7. The study showed that non-LTE effects lead to systematically depleted total absorption in the Pb I lines with ΔNLTE of the Pb I line at 4057.807 to be between 0.2 and 0.45 dex. This resulted in positive abundance corrections with departures from LTE increasing with decreasing metallicity. However, most of the stars considered in [47] were much cooler and with a higher surface gravity than that of the post-AGB stars. Therefore, dedicated non-LTE studies for post-AGB stars are critical to accurately investigate departures from LTE, especially for the derived Pb upper limits.

From a theoretical point of view, recent studies have revealed the possibility of an intermediate neutron-capture process, i.e., the *i*-process as a likely explanation for the abundance pattern observed in post-AGB stars enriched with the expected *s*-process elements. Other physical processes such as rotation, internal gravity wave mixing, and mass-loss prior to or during the AGB phase could also have strong impacts on the synthesis of elements, especially the neutron-capture elements.

Our current studies (see Section 3 and Kamath et al., 2021, to-be-submitted) present an increased sample of post-AGB objects, with well constrained luminosities (and hence initial masses) and metallicities, which show *i*-process abundance patterns, providing new possibilities to systematically test the mechanisms that induce *i*-process nucleosynthesis.

Author Contributions: Both authors contributed substantially to the conceptualization, composition, editing and revision of this manuscript. All authors have read and agreed to the published version of the manuscript.

Funding: DK acknowledges support from the Australian Research Council through DECRA grant number DE190100813. This research was supported in part by the Australian Research Council Centre of Excellence for All Sky Astrophysics in 3 Dimensions (ASTRO 3D) through project number CE170100013. HVW acknowledges support from the Research Council of the KU Leuven under grant number C14/17/082.

Acknowledgments: Both authors are grateful to the editor(s) of this special journal issue for the invitation to contribute this special feature article.

Conflicts of Interest: The authors declare no conflict of interest.

Appendix A

Table A1. Abundance ratios ([s/Fe], [Pb_{up}/hs], [Pb_{up}/ls]) and metallicities of the *s*-process rich single stars considered in this study, together with their effective temperature, and photospheric luminosities. See text for more details.

Object	Name	[Fe/H]	[s/Fe]	[Pb_{up}/hs]	[Pb_{up}/ls]	T_{eff}(K)	L/$L_\odot$
			Galaxy				
1	IRAS 05113+1347	-0.49 ± 0.15	1.54 ± 0.07	<-0.21	<0.11	5500	2000^{4700}_{1000}
2	IRAS 05341+0852	-0.54 ± 0.11	2.12 ± 0.05	<-0.14	<0.23	6750	300^{300}_{100}
3	IRAS 06530-0213	-0.32 ± 0.11	1.94 ± 0.06	<0.69	<0.98	7375	4700^{3500}_{2000}
4	IRAS 07134+1005	-0.91 ± 0.20	1.63 ± 0.14	<0.38	<0.37	7250	5500^{600}_{500}

Table A1. *Cont.*

Object	Name	[Fe/H]	[s/Fe]	[Pb_{up}/hs]	[Pb_{up}/ls]	T_{eff}(K)	L/$L_{\odot}$
5	IRAS 07430+1115	-0.31 ± 0.15	1.47 ± 0.06	<-0.48	<-0.23	6000	20^{10}_{10}
6	IRAS 08143-4406	-0.43 ± 0.11	1.65 ± 0.05	<0.32	<0.13	7000	4500^{1000}_{600}
7	IRAS 08281-4850	-0.26 ± 0.11	1.58 ± 0.09	<1.13	<1.14	7875	9600^{7100}_{4000}
8	IRAS 13245-5036	-0.30 ± 0.10	1.88 ± 0.09	<0.91	<1.38	9500	11200^{5600}_{4100}
9	IRAS 14325-6428	-0.56 ± 0.10	1.30 ± 0.14	<1.27	<1.35	8000	4900^{2100}_{1100}
10	IRAS 14429-4539	-0.18 ± 0.11	1.41 ± 0.08	<1.36	<1.54	9375	5000^{9600}_{3400}
11	IRAS 19500-1709	-0.59 ± 0.10	1.35 ± 0.21	<1.38	<1.35	8000	7100^{1000}_{900}
12	IRAS 22223+4327	-0.30 ± 0.11	1.03 ± 0.05	<0.94	<0.48	6500	5700^{400}_{500}
13	IRAS 22272+5435	-0.77 ± 0.12	1.80 ± 0.05	<-0.18	<0.11	5750	7700^{1700}_{1300}
			Small Magellanic Cloud				
14	J004441.04-732136.4	-1.34 ± 0.32	2.70 ± 0.30	<0.00	<0.52	6250	7600^{200}_{200}
			Large Magellanic Cloud				
15	J050632.10-714229.8	-1.22 ± 0.18	1.33 ± 0.30	<0.45	<0.10	6750	5400^{700}_{700}
16	J052043.86-692341.0	-1.15 ± 0.20	1.82 ± 0.25	<-0.45	<-0.27	5750	8700^{1000}_{1000}
17	J053250.69-713925.8	-1.22 ± 0.19	1.99 ± 0.25	<-0.24	<0.19	5500	6500^{100}_{100}
18	J051213.81-693537.1	-0.56 ± 0.15	1.61 ± 0.06	<0.37	<0.78	5875	6700^{200}_{200}
19	J051848.86-700246.9	-1.03 ± 0.14	1.90 ± 0.07	<-0.19	<0.47	6000	6250^{200}_{200}

The [Fe/H], [s/Fe], [Pb_{up}/hs], [Pb_{up}/ls], and T_{eff} results are taken from [25]. The luminosities, derived using the Gaia EDR3 parallaxes, are taken from Kamath et al., 2021, to-be-submitted. See Section 3 for more details.

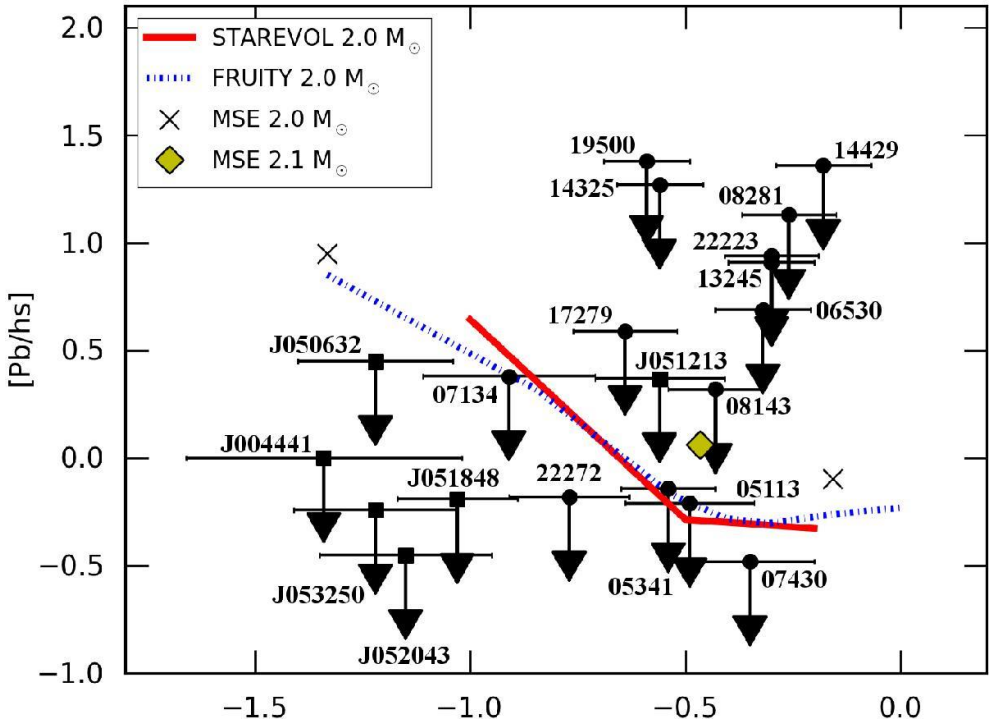

Figure A1. *Cont.*

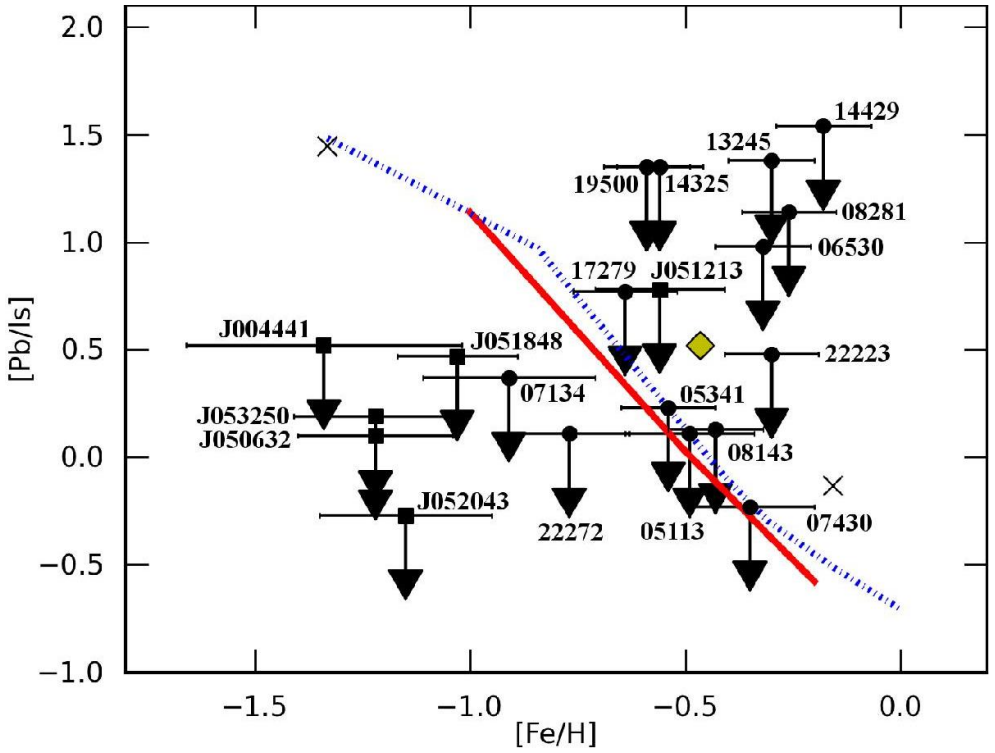

Figure A1. A reproduction of Figure 14 from [25]. The figure shows the observed [Pb_{up}/hs] (upper panel) and the [Pb_{up}/ls] (lower panel) versus [Fe/H] results of the sample of stars considered in [25]. The observed abundance upper limits are plotted together with the predictions of the STAREVOL models [38], Mount Stromlo models [36], and FRUITY models [42]. The black horizontal lines represent the [Fe/H] uncertainty of the displayed stars. See Section 3 and [25] for more details.

References

1. Buridge, E.M.; Burbidge, G.R. Chemical Composition of the BA II Star HD 46407 and its Bearing on Element Synthesis in Stars. *Astrophys. J.* **1957**, *126*, 357. [CrossRef]
2. Gallino, R.; Arlandini, C.; Busso, M.; Lugaro, M.; Travaglio, C.; Straniero, O.; Chieffi, A.; Limongi, M. Evolution and Nucleosynthesis in Low-Mass Asymptotic Giant Branch Stars. II. Neutron Capture and the s-Process. *Astrophys. J.* **1998**, *497*, 388. [CrossRef]
3. Goriely, S.; Mowlavi, N. Neutron-capture nucleosynthesis in AGB stars. *Astron. Astrophys.* **2000**, *362*, 599–614.
4. Lugaro, M.; Campbell, S.W.; Van Winckel, H.; De Smedt, K.; Karakas, A.I.; Käppeler, F. Post-AGB stars in the Magellanic Clouds and neutron-capture processes in AGB stars. *Astron. Astrophys.* **2015**, *583*, A77. [CrossRef]
5. Roederer, I.U.; Kratz, K.; Frebel, A.; Christlieb, N.; Pfeiffer, B.; Cowan, J.J.; Sneden, C. The End of Nucleosynthesis: Production of Lead and Thorium in the Early Galaxy. *Astrophys. J.* **2009**, *698*, 1963–1980. [CrossRef]
6. Cowan, J.J.; Sneden, C.; Lawler, J.E.; Aprahamian, A.; Wiescher, M.; Langanke, K.; Martínez-Pinedo, G.; Thielemann, F.K. Origin of the heaviest elements: The rapid neutron-capture process. *Rev. Mod. Phys.* **2021**, *93*, 015002. [CrossRef]
7. Merrill, S.P.W. Spectroscopic Observations of Stars of Class S. *ApJ* **1952**, *116*, 21–26. [CrossRef]
8. Iben, I., Jr. *Asymptotic Giant Branch Stars: Thermal Pulses, Carbon Production, and Dredge Up; Neutron Sources and S-Process Nucleosynthesis*; IAU Symp. 145: Evolution of Stars: The Photospheric Abundance Connection; Michaud, G., Tutukov, A.V., Eds.; Cambridge University Press: Cambridge, UK, 1991; p. 257.
9. Busso, M.; Gallino, R.; Wasserburg, G.J. Nucleosynthesis in Asymptotic Giant Branch Stars: Relevance for Galactic Enrichment and Solar System Formation. *Annu. Rev. Astron. Astrophys.* **1999**, *37*, 239–309. [CrossRef]
10. Herwig, F. Evolution of Asymptotic Giant Branch Stars. *Annu. Rev. Astron. Astrophys.* **2005**, *43*, 435–479. [CrossRef]
11. Lugaro, M.; Karakas, A.I.; Stancliffe, R.J.; Rijs, C. The s-process in Asymptotic Giant Branch Stars of Low Metallicity and the Composition of Carbon-enhanced Metal-poor Stars. *Astrophys. J.* **2012**, *747*, 2. [CrossRef]
12. Karakas, A.I.; Lattanzio, J.C. The Dawes Review 2: Nucleosynthesis and Stellar Yields of Low- and Intermediate-Mass Single Stars. *Publ. Astron. Soc. Aust.* **2014**, *31*, e030. [CrossRef]
13. Van Eck, S.; Goriely, S.; Jorissen, A.; Plez, B. Discovery of three lead-rich stars. *Nature* **2001**, *412*, 793–795. [CrossRef] [PubMed]
14. Aoki, W.; Ryan, S.G.; Norris, J.E.; Beers, T.C.; Ando, H.; Tsangarides, S. A Subaru/High Dispersion Spectrograph Study of Lead (Pb) Abundances in Eight s-Process Element-rich, Metal-poor Stars. *Astrophys. J.* **2002**, *580*, 1149–1158. [CrossRef]
15. Van Eck, S.; Goriely, S.; Jorissen, A.; Plez, B. More lead stars. *Astron. Astrophys.* **2003**, *404*, 291–299. [CrossRef]

16. Cowan, J.J.; Rose, W.K. Production of ^{14}C and neutrons in red giants. *Astrophys. J.* **1977**, *212*, 149–158. [CrossRef]
17. Siess, L.; Livio, M.; Lattanzio, J. Structure, Evolution, and Nucleosynthesis of Primordial Stars. *Astrophys. J.* **2002**, *570*, 329–343. [CrossRef]
18. Campbell, S.W.; Lattanzio, J.C. Evolution and nucleosynthesis of extremely metal-poor and metal-free low- and intermediate-mass stars. I. Stellar yield tables and the CEMPs. *Astron. Astrophys.* **2008**, *490*, 769–776. [CrossRef]
19. Hampel, M.; Karakas, A.I.; Stancliffe, R.J.; Meyer, B.S.; Lugaro, M. Learning about the Intermediate Neutron-capture Process from Lead Abundances. *Astrophys. J.* **2019**, *887*, 11. [CrossRef]
20. Roederer, I.U.; Cowan, J.J.; Karakas, A.I.; Kratz, K.; Lugaro, M.; Simmerer, J.; Farouqi, K.; Sneden, C. The Ubiquity of the Rapid Neutron-capture Process. *Astrophys. J.* **2010**, *724*, 975–993. [CrossRef]
21. Beers, T.C.; Christlieb, N. The Discovery and Analysis of Very Metal-Poor Stars in the Galaxy. *Annu. Rev. Astron. Astrophys.* **2005**, *43*, 531–580. [CrossRef]
22. Bisterzo, S.; Gallino, R.; Straniero, O.; Cristallo, S.; Käppeler, F. s-Process in low-metallicity stars-I. Theoretical predictions. *Mon. Not. R. Astron. Soc.* **2010**, *404*, 1529–1544. [CrossRef]
23. Abate, C.; Stancliffe, R.J.; Liu, Z.W. How plausible are the proposed formation scenarios of CEMP-r/s stars? *Astron. Astrophys.* **2016**, *587*, A50. [CrossRef]
24. Karinkuzhi, D.; Van Eck, S.; Goriely, S.; Siess, L.; Jorissen, A.; Merle, T.; Escorza, A.; Masseron, T. Low-mass low-metallicity AGB stars as an efficient i-process site explaining CEMP-rs stars. *Astron. Astrophys.* **2021**, *645*, A61. [CrossRef]
25. De Smedt, K.; Van Winckel, H.; Kamath, D.; Siess, L.; Goriely, S.; Karakas, A.I.; Manick, R. Detailed homogeneous abundance studies of 14 Galactic s-process enriched post-AGB stars: In search of lead (Pb). *Astron. Astrophys.* **2016**, *587*, A6. [CrossRef]
26. De Smedt, K.; Van Winckel, H.; Kamath, D.; Wood, P.R. Chemical abundance study of two strongly s-process enriched post-AGB stars in the LMC: J051213.81-693537.1 and J051848.86-700246.9. *Astron. Astrophys.* **2015**, *583*, A56. [CrossRef]
27. Mowlavi, N.; Meynet, G. Aluminum 26 production in asymptotic giant branch stars. *Astron. Astrophys.* **2000**, *361*, 959–976.
28. Bailer-Jones, C.A.L.; Rybizki, J.; Fouesneau, M.; Demleitner, M.; Andrae, R. VizieR Online Data Catalog: Distances to 1.47 billion stars in Gaia EDR3 (Bailer-Jones+, 2021). *VizieR Online Data Catalog* **2021**, I/352. Available online: https://ui.adsabs.harvard.edu/abs/2021yCat.1352....0B/abstract (accessed on 1 November 2021).
29. Reyniers, M.; Van Winckel, H. Detection of elements beyond the Ba-peak in VLT+UVES spectra of post-AGB stars. *Astron. Astrophys.* **2003**, *408*, L33–L37. [CrossRef]
30. Abia, C.; de Laverny, P.; Wahlin, R. Chemical analysis of carbon stars in the Local Group. II. The Carina dwarf spheroidal galaxy. *Astron. Astrophys.* **2008**, *481*, 161–168. [CrossRef]
31. Van Winckel, H. Post-Agb Stars. *Annu. Rev. Astron. Astrophys.* **2003**, *41*, 391–427. [CrossRef]
32. Kamath, D.; Wood, P.R.; Van Winckel, H. Optically visible post-AGB/RGB stars and young stellar objects in the Small Magellanic Cloud: Candidate selection, spectral energy distributions and spectroscopic examination. *Mon. Not. R. Astron. Soc.* **2014**, *439*, 2211–2270. [CrossRef]
33. van Aarle, E.; Van Winckel, H.; Lloyd Evans, T.; Ueta, T.; Wood, P.R.; Ginsburg, A.G. The optically bright post-AGB population of the LMC. *Astron. Astrophys.* **2011**, *530*, A90. [CrossRef]
34. Kamath, D.; Wood, P.R.; Van Winckel, H. Optically visible post-AGB stars, post-RGB stars and young stellar objects in the Large Magellanic Cloud. *Mon. Not. R. Astron. Soc.* **2015**, *454*, 1468–1502. [CrossRef]
35. De Smedt, K. The Chemical Diversity of Post-AGB Stars in the Galaxy and the Magellanic Clouds. Ph.D. Thesis, Institute of Astronomy, KU Leuven, Leuven, Belgium, 2015.
36. Siess, L. Evolution of massive AGB stars. II. model properties at non-solar metallicity and the fate of Super-AGB stars. *Astron. Astrophys.* **2007**, *476*, 893–909. [CrossRef]
37. Cristallo, S.; Straniero, O.; Gallino, R.; Piersanti, L.; Domínguez, I.; Lederer, M.T. Evolution, Nucleosynthesis, and Yields of Low-Mass Asymptotic Giant Branch Stars at Different Metallicities. *Astrophys. J.* **2009**, *696*, 797–820. [CrossRef]
38. Fishlock, C.K.; Karakas, A.I.; Lugaro, M.; Yong, D. Evolution and Nucleosynthesis of Asymptotic Giant Branch Stellar Models of Low Metallicity. *Astrophys. J.* **2014**, *797*, 44. [CrossRef]
39. De Smedt, K.; Van Winckel, H.; Karakas, A.I.; Siess, L.; Goriely, S.; Wood, P.R. Post-AGB stars in the SMC as tracers of stellar evolution: The extreme s-process enrichment of the 21 μm star J004441.04-732136.4. *Astron. Astrophys.* **2012**, *541*, A67. [CrossRef]
40. Goriely, S.; Siess, L. S-process in hot AGB stars: A complex interplay between diffusive mixing and nuclear burning. *Astron. Astrophys.* **2004**, *421*, L25–L28. [CrossRef]
41. Cristallo, S.; Piersanti, L.; Straniero, O.; Gallino, R.; Domínguez, I.; Abia, C.; Di Rico, G.; Quintini, M.; Bisterzo, S. Evolution, Nucleosynthesis, and Yields of Low-mass Asymptotic Giant Branch Stars at Different Metallicities. II. The FRUITY Database. *Astrophys. J. Suppl. Ser.* **2011**, *197*, 17. [CrossRef]
42. Cristallo, S.; Straniero, O.; Piersanti, L.; Gobrecht, D. Evolution, Nucleosynthesis, and Yields of AGB Stars at Different Metallicities. III. Intermediate-mass Models, Revised Low-mass Models, and the ph-FRUITY Interface. *Astrophys. J. Suppl. Ser.* **2015**, *219*, 40. [CrossRef]
43. Choplin, A.; Siess, L.; Goriely, S. The intermediate neutron capture process. I. Development of the i-process in low-metallicity low-mass AGB stars. *Astron. Astrophys.* **2021**, *648*, A119. [CrossRef]
44. Cristallo, S.; Karinkuzhi, D.; Goswami, A.; Piersanti, L.; Gobrecht, D. Constraints of the Physics of Low-mass AGB Stars from CH and CEMP Stars. *Astrophys. J.* **2016**, *833*, 181. [CrossRef]

45. Denissenkov, P.A.; Herwig, F.; Woodward, P.; Andrassy, R.; Pignatari, M.; Jones, S. The i-process yields of rapidly accreting white dwarfs from multicycle He-shell flash stellar evolution models with mixing parametrizations from 3D hydrodynamics simulations. *Mon. Not. R. Astron. Soc.* **2019**, *488*, 4258–4270. [CrossRef]
46. De Smedt, K.; Van Winckel, H.; Kamath, D.; Karakas, A.I.; Siess, L.; Goriely, S.; Wood, P. The lead discrepancy in intrinsically s-process enriched post-AGB stars in the Magellanic Clouds. *Astron. Astrophys.* **2014**, *563*, L5. [CrossRef]
47. Mashonkina, L.; Ryabtsev, A.; Frebel, A. Non-LTE effects on the lead and thorium abundance determinations for cool stars. *Astron. Astrophys.* **2012**, *540*, A98. [CrossRef]